Oceanologia, uncorrected, in press
Polish Academy of Sciences
Institute of Oceanology

https://doi.org/10.5697/...

Seabed saturation conditions from in-situ measurements performed on Norderney

Waldemar Magda

Abstract
This paper deals with an important coastal engineering problem of defining proper seabed saturation conditions, which have a significant influence on the pore-fluid compressibility and the wave-induced cyclic response of poro-elastic seabed sediments. A unique in-situ measuring campaign was conducted in the tidal zone of the northern beach of Norderney, off the North Sea coast of Germany, where 186 sandy seabed samples were taken underwater. Based on the laboratory measurements, a set of calculated saturation degrees was statistically analyzed. Both the histogram and the normal Q-Q plot, as well as the Shapiro-Wilk normality test, confirmed the validity of the assumption of the normal probability distribution for the variability of the degree of saturation. The mean degree of saturation of the top layer of the se usabed, $(\overline{S}_r) = 0.973$, constitutes the main output of the study, whereas the uncertainty propagation analysis enabled to define the possible range of variation, which is $0.962 \leq (\overline{S}_r) \leq 0.986$. It should be clearly emphasised that a proper assessment of the seabed saturation conditions is very important, mainly due to the correctness of the description of the wave-induced pore-fluid pressure field used in more detailed analyses of the pore-fluid pressure gradients and the liquefaction potential of the seabed, which have a direct impact on phenomena such as sand transport on beaches, seabed erosion, and stability of coastal structures (e.g. breakwaters and submarine buried pipelines).

Keywords
Coastal engineering; Intertidal zone; Partly saturated seabed; Degree of saturation; In-situ seabed sampling; Statistical analysis

Department of Geotechnical and Hydraulic Engineering, Gdańsk University of Technology, 11/12 Gabriela Narutowicza Street, 80-233 Gdańsk, Poland
***Correspondence**: waldemar.magda@pg.edu.pl

Received: 13 July 2025; **revised:** 18 January 2026; **accepted**: 23 February 2026

1. Introduction

Many more advanced solutions for the prediction of the wave-induced cyclic seabed response (by means of the pore-fluid pressure and stresses in the soil matrix) are strongly dependent on the compressibility of the two-phase (pore-fluid and soil skeleton) seabed medium. The pore-fluid is treated as a mixture of seawater and air entrapped in pores of seabed sediments in the form of occluded micro air bubbles. The relationship between the amount of free air in the pore-fluid, represented by the degree of saturation, and the compressibility of the pore-fluid can be given by a common and very practical formula proposed by Verruijt (1969). This relationship has been used for decades by many researchers, among others: Madsen (1978), Yamamoto et al. (1978), Nago and Maeno (1984), Okusa (1985), Magda (1994, 1998), Hsu and Jeng (1994), Jeng (2013, 2018), indicating a very strong dependence of the wave-induced pore-fluid cyclic response on seabed saturation conditions. The degree of saturation plays a very important role in the process of pore-fluid pressure generation, both cyclic and residual, within seabed sediments. Therefore, this geotechnical parameter has a great bearing on many applications in coastal and offshore engineering. Any changes in the degree of saturation, even by a relatively small increment, in the range that is supposed to be found under natural conditions, mainly due to a certain inhomogeneity of seabed sediments, cause significant changes in the pore-fluid compressibility, particularly when the degree of saturation is close to unity (almost fully saturated seabed conditions).

What is the real value of the degree of saturation characterising seabed sediments? It is a difficult question remaining open. Inhomogeneity of seabed sediments and difficulties with very precise seabed sampling make the problem even worse. Many researchers (Table 1), when conducting analytical and numerical analyses of the wave-induced cyclic seabed response, prefer doing parametric

Table 1. A list (in chronological order) of some selected past research works using particular values of the degree of saturation, S_r, assumed in different analyses of the wave-induced seabed response.

Author/Authors	S_r [–]	Remarks
Madsen (1978)	0.965–1.0	Assumed in the parametric study.
Yamamoto et al. (1978)	0.95–1.0	Assumed in the parametric study.
	0.98	Obtained from the experiment by matching with the equation by Verruijt (1969).
Mei and Foda (1981)	0.92	Assumed as typical for the North Sea condition, recalculated from $G\beta = 10^4$ by Magda (2025).
Nago and Maeno (184)	0.993	Assumed indirectly by taking the water and air porosities: $\lambda_w = 0.4$ and $\lambda_a = 0.003$, respectively.
Okusa (1985)	0.93–1.0	Assumed indirectly for loose sand by taking Skempton's pore-water coefficient B = 0.5 − 1.0.
	0.95–1.0	Assumed indirectly for dense sand by taking Skempton's pore-water coefficient B = 0.5 − 1.0.
Hsu and Jeng (1994)	0.966	Obtained by matching with the boundary-layer approximation by Mei and Foda (1981).
Ulker and Rahman (2009)	1.0	Assumed in the numerical experiments on the inertia effects.
Merxhani and Liang (2012)	1.0	Assumed in the analysis of the seabed response due to solitary waves.
Jeng (2013, 2018)	0.932	Obtained by matching with the boundary-layer approximation by Mei and Fora (1981).
Sumer (2014)	1.0	Assumed in the assessment of liquefaction potential.
	0.985	Assumed in the momentary liquefaction analysis.

studies with respect to the degree of saturation rather than performing demanding research for the degree of saturation typical for the case under consideration. This leads very often to presentations of the main computational results achieved for a wide range of possible values of S_r. Usually, this way of doing is fully justified and very desirable when presenting abilities of a newly derived analytical solution or looking for an optimum/maximum particular solution, as it is the case, for example, when the maximum uplift force acting on a submarine pipeline buried in seabed sediments is sought (Magda, 1992, 1997, 2000). It also happens that the researchers assume fully saturated soil conditions ($S_r = 1$) for the purpose of their analyses without giving any grounds for so doing. It is worth noting that only a few of the researchers reported some values of S_r measured in seabed sediments under natural conditions (Table 2).

Some other researchers try to match the results of their own computations with previously published results of other authors by selecting a suitable value of the degree of saturation, which is a kind of back analysis. As typical examples thereof, the works by Hsu and Jeng (1994) and Jeng (2013, 2018) can be cited. Unfortunately, in this particular case, such action turned out to be disastrous, leading to questionable results. Hsu and Jeng (1994) and Jeng (2013, 2018) made many efforts in trying to replicate the seabed response results, obtained by means of pore-fluid pressure, soil displacements, and stresses, and published by Mei and Foda (1981) for the North Sea wave and seabed conditions, by applying their own analytical solutions. Unfortunately, they failed because multiple recalculations of one and the same case of the wave-induced seabed response required the usage of different values of the degree of saturation: $S_r = 0.966$ (Hsu and Jeng, 1994), $S_r = 0.932$ (Jeng, 2013, 2018), which, of course, cannot be acceptable. In addition, the author of the present paper made his own computations, using the analytical solution derived personally (Magda, 1994; Richwien and Magda,

Table 2. A short list (in chronological order) of some selected past research works reporting particular values of the degree of saturation, S_r, based on in-situ measurements.

Author / Authors	S_r [–]	Remarks
Sandven et al. (2007)	0.988–1.0	Measured under falling (ebbing) tide conditions after repeated cycles of strong waves
Tørum (2007)	0.97	Calculated by matching the field data with the boundary-layer theory by Mei and Foda (1981).
Michallet et al. (2009)	0.94–1.0	Calculated from the image analysis of the geoendoscopic video camera recording (minimum at a depth of 0.2–0.3 m)

1994), and the matching point was indicated for the degree of saturation to be equal to $S_r = 0.920$ (Magda, 2025). All together, there are three different values of S_r describing one and the same case! This particular bizarre example of extremely different values of the degree of saturation describing one and the same case can only emphasise the need for further investigations proving the real values of the degree of saturation under natural conditions. It seems that the authors of some research papers are freely juggling different values of the degree of saturation, having no well-established idea at what level the actual seabed saturation conditions may develop.

1.1 Objectives of the research

The main motivation of this research paper is to get a better insight into the problem of real saturation conditions by means of in-situ seabed sampling. A basic task of the research paper is to present the results of a unique measuring campaign performed on the northern beach of Norderney in order to gather samples of the upper seabed layer undergoing tidal movements. The results of laboratory measurements and additional calculations should give important statistics of the degree of saturation characterising natural environmental conditions that can be found in intertidal beach regions.

2. In-situ measuring campaign

The scientific expedition to Norderney, an island off the North Sea coast of Germany, was organised and conducted as a part of the scientific programme TP-A13 'Cyclic and transient wave-induced loading of the seabed' (in German: 'Transiente und zyklische Beanspruchung von Böden durch Seegang') within the frame of the Coastal Engineering Research Programme (in German: Sonderforschungsbereich – 205 'Küsteningenieurwesen'). The main purpose of the expedition was to collect many samples of the upper part of the seabed sandy sediments by performing in-situ sampling followed by laboratory measurements in order to evaluate the degree of saturation existing under the natural environmental conditions of the tidal region of Norderney.

Norderney (Figure 1) is one of the seven populated East Frisian Islands and part of the Lower Saxony Land (state). The island is 13 km long and up to 2 km wide, with dunes rising to 21 metres. The northern coast is exposed to the sea. During low tide, the beach width can reach 550 m. The beach comprises well-sorted quartz fine sand with a median grain size of $d_{50} = 218\ \mu$m (Eichmanns and Schüttrumpf, 2021). Norderney has a mean tidal range of approximately 2.4 m, which stays within the mesotidal range. The annual mean significant wave height varies from 0.7 m to 1.0 m (Niemeyer, 1992).

A particular place chosen for the seabed sampling is marked in Figure 1. The sampling site was located on the northern beach of Norderney. The sampling was preceded by geodetic measurements, as a result of which a vertical cross-section of the beach along the sampling line was obtained (Figure 2). The zone of seabed sampling was located within the tidal (intertidal) range, i.e., between the High Tide (HT) and the Low Tide (LT) levels of sea water tidal movements. The extreme locations of the sampling points, obtained with respect to the vertical datum of the Mean Sea Level (MSL), had the following abscissas and elevations: $x = 70$ m and $y = 1.21$ m for Point 2 and $x = 415$ m and $y = -1.10$ m for Point 30 (see Figure 2). The total length of the sampling zone was equal to 345 m, which implies that the mean intertidal beach slope was rather mild, with the average inclination $m = [1.21 - (-1.10)]/345.0 \cong 0.0067 \cong 1 : 150$.

2.1 Procedure of seabed sampling

During the sampling campaign, 186 samples of sandy seabed sediments were taken underwater during different phases of the tidal water motion (see Figure 2):

- Day 1, series 1, phase of ebbing, sample nos. 1–38 (38 samples).
- Day 2, series 2, phase of flooding, sample nos. 39-78 (40 samples).
- Day 2, series 3, phase of ebbing, sample nos. 79–127 (49 samples).
- Day 3, series 4, phase of flooding, sample nos. 128–186 (59 samples).

The beginning of sampling started approximately at one of the extreme water levels, i.e., either the High Tide

Figure 1. Aerial view of Norderney, indicating the place of seabed sampling (based on Wikipedia.com (2025)).

(HT) or the Low Tide (LT), and was performed stepwise during the ebbing or flooding phases of the tidal movement, respectively, when the water level was moving towards another extreme position. All the samples were taken when the seabed surface at the sampling point was below the actual water level. The water depth at the sampling point was always kept equal to approximately 0.1–0.2 m. A smaller depth could cause some losses of water within the sand sample during its 'excavation' from the seabed, and because of existing small waves, it could not produce permanent underwater conditions for the surface of the sampling area. On the other hand, a bigger water depth could cause difficulties in the sampling procedure, as it would be more difficult to bring the whole undisturbed (i.e., naturally saturated) sandy sample above the water surface. The subsequent sampling points followed the water line's actual positions.

The sampling device used in the procedure consisted of the following three tools made of aluminium: a sampling cylinder, a circular plate with a guiding cylinder, and a piston. A perforated upper surface of the piston protected against the creation of artificial and disturbing filtration of seawater through the soil sample when the sampling cylinder was slowly pressed down by the piston into the seabed. After pressing the sampling cylinder into the seabed (made using the guiding cylinder and the piston) and levelling the upper surface of the sand sample, the top of the cylinder was slowly capped. Then, digging out the sample was performed at a slow rate in order to avoid the suction effect on the sample. At the end, the sample was lifted above the water level and simultaneously turned upside-down to preserve the natural water content within the sample and to allow the levelling of the sand surface from the other side of the sample. Just after extracting from the seabed, the sampling cylinder was emptied carefully and precisely, and single soil samples were stored alone in separate, identical plastic and hermetic containers. Afterwards, all the containers, together with the wet sand samples inside, were weighed one by one, and then, they were dried in a dryer (temperature of 105°C applied for 24 hours). At the end of the laboratory procedure, the dry sand samples and the respective dry containers were weighed.

2.2 Governing equations

Directly, the following parameters were measured (weighed) at the laboratory: total mass of wet sample (sand sample plus container), $m_{w(s+c)}$ [g], mass of dry container, m_{dc} [g], and mass of dry sand sample, m_{ds} [g]. Consequently, it became possible to measure the mass of the wet soil sample, m_{ws} [g], and the mass of water in the sample, m_w [g]:

$$m_{ws} = m_{w(s+c)} - m_{dc} = \rho_{ws} V_t \tag{1a}$$

$$m_w = m_{ws} - m_{ds} \tag{1b}$$

and the rest of the required parameters:

$$V_w = \frac{m_w}{\rho_{sw}} \tag{1c}$$

$$V_s = \frac{m_{ds}}{G_s \rho_w} \tag{1d}$$

$$V_v = V_t - V_s \tag{1e}$$

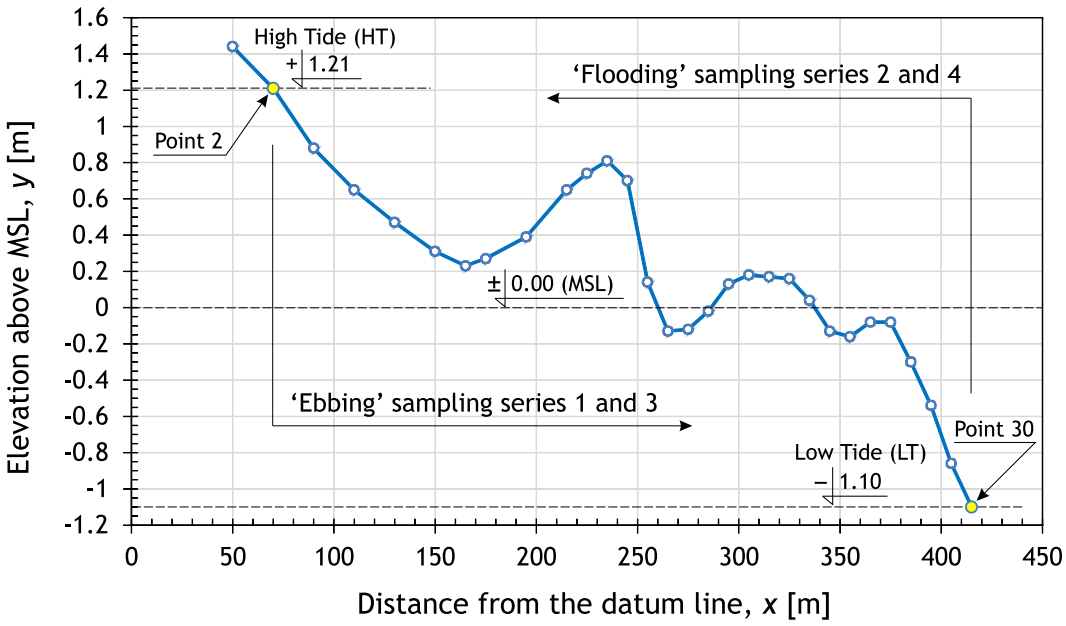

Figure 2. Vertical profile of Norderney beach in the sampling line within the intertidal range of water surface movement.

where, additionally: V_w is the volume of water in the sample [cm^3], V_s is the volume of solid soil particles [cm^3], V_v is the volume of voids in the soil skeleton [cm^3], V_t is the total volume of the soil sample [cm^3], G_s is the specific gravity of the soil particles (defined with respect to the density of pure water, ρ_w, at temperature 20°C) [–], ρ_{ws} is the density of the wet sample [g/cm^3], ρ_w is the density of pure water [g/cm^3], ρ_{sw} is the density of seawater [g/cm^3].

Using the basic definition of the degree of saturation (Craig, 2004)

$$S_r \overset{\text{def}}{=} \frac{V_w}{V_v} \tag{2}$$

taking Eqs. (1a)–(1e) together with Eq. (2), and performing some mathematical operations, it was possible to derive the following practical form of the equation for the degree of saturation

$$S_r = \frac{m_{w(s+c)} - m_{dc} - m_{ds}}{\rho_w V_t - \frac{m_{ds}}{G_s}} \times \frac{\rho_w}{\rho_{ws}} \tag{3}$$

As indicated in Eq. (3), five measured parameters ($m_{w(s+c)}$, m_{dc}, m_{ds}, G_s, and V_t) must be known to calculate the degree of saturation, S_r. Each weighing carried out with respect to $m_{w(s+c)}$ and m_{ds} was performed with the instrument accuracy (weighing precision or readability) of $\Delta m_{w(s+c)} = \Delta m_{ds} = 0.5$ g (a scale ballance – accuracy is equal to the smallest increment divided by 2), whereas the instrument accuracy for measurements of m_{dc} was equal to $\Delta m_{dc} = 0.1$ g (a digital display electronic balance – accuracy is equal to the smallest increment).

The specific gravity of soil was measured using the pycnometer technique and calculated according to the following relation

$$G_s = \frac{m_2 - m_1}{(m_4 - m_1) - (m_3 - m_2)} \tag{4}$$

where: G_s is the specific gravity of soil solids [–], m_1 is the mass of the pycnometer [g], m_2 is the mass of the pycnometer plus soil [g], m_3 is the mass of the pycnometer plus soil plus pure (distilled) water [g], m_4 is the mass of the pycnometer plus pure (distilled) water [g]. The specific gravity of the soil particles at 20°C was found to be $G_s = 2.654$ (typical for quartz-type sand), calculated as the mean from 8 samples randomly selected (2 samples per each of 4 series) from the whole group of 186 seabed samples. The laboratory measurements of G_s were performed using the pycnometer bottle technique, and the component masses were measured with the instrument accuracy equal to $\Delta m_1 = \Delta m_2 = \Delta m_3 = \Delta m_4 = 0.1$ g (a digital display electronic balance). According to the geotechnical practice, values of G_s are usually rounded to the nearest 0.01 (rounding to the nearest 0.001 is used in the present study).

The total volume of the sample is the same as the volume of the sampling cylinder, which was calculated using the following simple equation

$$V_t \equiv V_c = \frac{\pi D_i^2}{4} h \tag{5}$$

where: V_t is the total volume of the seabed sample [cm^3], V_c is the volume of the sampling cylinder [cm^3], D_i is the

inside diameter of the sampling cylinder [cm], h is the height of the sampling cylinder [cm]. The geometry of the sampling cylinder was measured only once, leading to the following dimensions: the outside diameter $D_i = 9.85$ cm, the inside diameter $D_i = 9.6$ cm, and the height $h = 12.0$ cm. These parameters imply the total volume of samples is equal to $V_t \equiv V_c = 868.59$ cm^3. The measurements of the cylinder geometry were performed using a digital caliper with the instrument accuracy equal to $\Delta D_i = \Delta h = 0.01$ cm. The disturbance surface ratio, which is the ratio of the material cross-sectional area to the outer cross-sectional area of the sampling cylinder, was equal to 5%, which is fully acceptable for that type of test, as far as possible meaningful disturbances during the cylinder pressing are taken into account.

The density of water, influenced by temperature, pressure, and salinity, was computed using very precise formulas presented by Gill (1982) and Kell (1975). The density of pure water, at the standard pressure $p_{at} = 101.325$ kPa and the standard temperature $t = 20$°C (applied for pycnometer measurements), was equal to $\rho_w = 998.21$ kg/m^3. The seawater temperature during the seabed sampling equaled $t = 6.8$°C, whereas the practical salinity of seawater, typical for the northern coastline of Norderney, is reported to be $S_p = 30$ with only a very small seasonal variability (Quante and Colijn, 2016). Taking it into account, the density of seawater was calculated to be $\rho_{sw} = 1023.51$ kg/m^3.

3. Statistical analysis of the measurements

3.1 Basic descriptive statistics

On the basis of the values measured in the laboratory and calculated for each seabed sample taken on Norderney, further data analysis was performed using a statistical approach, by applying the following four commonly accepted basic statistical parameters of the random variable x, defined with respect to a sample taken from the population: the mean (average), $\overline{x}$, the median, $\tilde{x}$, the standard deviation, $s(x)$, and the standard deviation of the mean, $s(\overline{x}) = s(x)/\sqrt{n}$ (n is the number of repeated measurements in the set). The descriptive statistics, applied to the measured and calculated parameters, obtained for the total group of 186 seabed samples, are presented in Table 3.

Table 3. Descriptive statistics for the basic parameters.

Parameter	Unit	Mean $\overline{x}$	Median $\overline{x}$	Standard deviation $s(x)$	Standard deviation of the mean $s(\overline{x})$
$m_{w(s+c)}$	[g]	1906.84	1908.0	23.54	1.73
m_{dc}	[g]	124.16	123.45	1.36	0.10
m_{ws} (Eq. (1a))	[g]	1782.67	1784.0	23.26	1.71
m_{ds}	[g]	1472.09	1472.0	22.78	1.67
G_s	[–]	2.654	2.654	0.008	0.003
S_r (Eq. (3))	[–]	0.973	0.974	0.045	0.003

3.2 Histograms

A histogram is a visual representation of the distribution of quantitative data. The total area of a histogram used for probability density is usually normalised to 1. A normalised number of samples can be calculated according to the following recipe

$$n_N = \frac{n_B}{n}\frac{s(x)}{B} \tag{6}$$

where: n_N is the normalised number of samples in a histogram bin, n_B is the number of samples in a histogram bin, n is the total number of samples, $s(x)$ is the standard deviation of a real-valued random variable x, B is the width of a histogram bin. In constructing histograms, for $n > 100$, it usually works well to use a maximum of about $10 \times \log_{10} n$ bins (Fox, 2016). In the present case of 186 samples, the condition $n = 186 > 100$ indicates that the number of bins should not exceed $10 \times \log_{10} 186 = 22.67 \cong 22$. In the case of the mass of the total wet sample, $m_{w(s+c)}$, the minimum and the maximum were equal to 1825.0 g and 1974.0 g, respectively. Covering the entire range from 1820.0 g to 1980.0 g with bins of the width $B = 10$ g, the total number of $n_B = 16$ bins is required. In the case of the degree of saturation, S_r, starting the histogram distribution from $S_r = 0.84$ and ending with $S_r = 1.12$, all the data were represented, including both the minimum and maximum values, $S_r = 0.848$ and $S_r = 1.112$, respectively. The range $S_r = 0.84 - 1.12$, together with the assumed bin width $B = 0.02$, implies $n_B = (1.12 - 0.84)/0.02 = 14$ bins. Both numbers of bins fulfil the above-given condition ($n_B \leq 22$).

Taking into account the initially measured parameter, which is the mass of the total wet sample (wet soil plus container), $m_(w(s+c))$, and the resulting calculated parameter, which is the degree of saturation, S_r, Figures 3 and 4 show the normalised histograms (highlighted by the green bins), of both parameters, respectively. The numbers placed at the bottom of each bin indicate the number of samples counted for a specific bin. As expected, according to visual assessment, the nomogram tends to follow the normal (Gaussian) probability distribution – this will be proved more precisely in the next paragraph, using formal normality tests. Moreover, the histogram of the degree of saturation, presented in Figure 4, seems to exhibit small asymmetries around its mean. This can be checked by evaluating skewness, which is the distribution's tendency to 'lean' to one side or the other of the mean. In statistics and probability theory, the non-parametric skew is a statistic occasionally used with random variables that take real values – it is a measure of the skewness of a random variable's distribution. Taking the histogram of the degree of saturation (see Figure 4), and the appropriate values given in

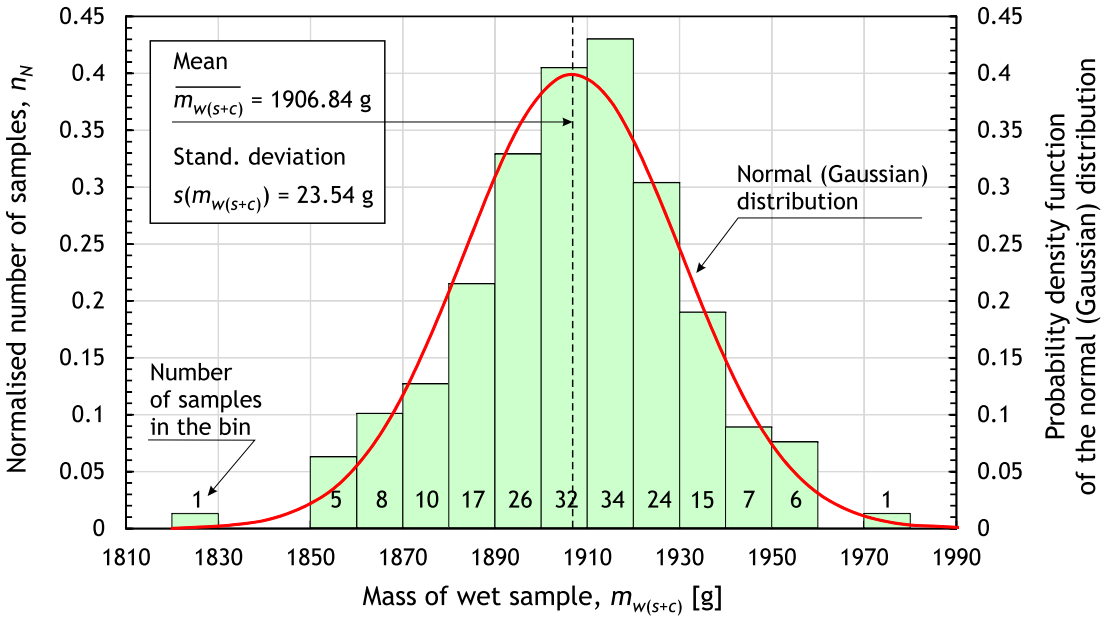

Figure 3. Normalised histogram of the mass of total wet sample (wet soil plus container), $m_{w(s+c)}$, overlaid by the normal (Gaussian) distribution of probability.

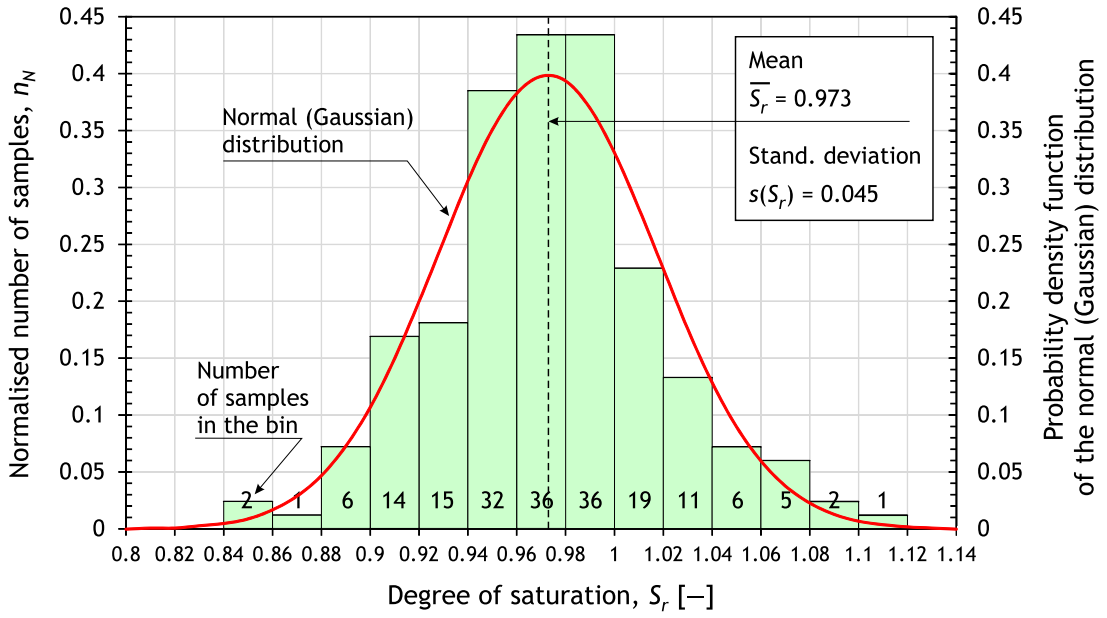

Figure 4. Normalised histogram of the degree of saturation, S_r, overlaid by the normal (Gaussian) distribution of probability.

Table 3, the nonparametric skew equals

$$S(S_r) = \frac{\overline{S}_r - \tilde{S}_r}{s(S_r)} = \frac{0.973 - 0.974}{0.045} = -0.022 \qquad (7)$$

Therefore, this type of distribution is said to be left-skewed and the distribution appears as a right-leaning curve, which means that the left tail of the distribution is longer than the right one (the mass of the distribution is concentrated on the right of the figure).

3.3 Tests on data normality

In statistics, normality tests are used to determine if a data set is well modelled by a normal distribution. In other

words, they check if the shape of the distribution under consideration is similar to the shape of the normal (Gaussian) distribution. One of the most powerful tests for normality is the Shapiro-Wilk (S-W) test and the d'Agostino-Pearson test. The so-called null hypothesis, H_0, of these tests is that the population is normally distributed. If the p-value is greater than a certain predefined significance level, then the null hypothesis is not rejected. The significance level is commonly set a priori to $\alpha = 0.05$.

The modification of the Shapiro-Wilk test, proposed by Royston (1982) for a large number of data ($n = 2000$), was used in the present work. In order to perform the S-W test, the program codes DERF.for and DIERFC.for (written in Fortran 77 by Ooura (1996)) were adapted to compute the error function and the inverse complementary error function, respectively. The main results of the normality tests are presented in Table 4.

For the random variable represented by the degree of saturation, S_r, the following test results were obtained: the test statistic $W = 0.988$ and the probability value $p = 0.134$. The probability value fulfils the condition $p > \alpha$; therefore, the null hypothesis can be accepted with only a 5% risk of a false positive conclusion. It means that there is evidence that the degree of saturation data tested can be treated as normally distributed. This finding was additionally proved by using another powerful normality test, that is the d'Agostino-Pearson test, from which the following test results were obtained: the test statistic $\chi^2 = 3.612$ and the probability value $p = 0.164$.

Unfortunately, the distribution of the mass of dry container, m_{dc}, failed the normality test (Shapiro-Wilk test: $W = 0.825$ and $p = 1.1 \times 10^{-13} \cong 0 < 0.05$; d'Agostino-Pearson test: $\chi^2 = 23.56$ and $p = 7.7 \times 10^{-6} \cong 0 < 0.05$). Firstly, this is due to meaningfully different masses of the sample containers, although they were believed to be identical. Secondly, the independence of the masses was corrupted entirely by accident and unknowingly, using the same set of containers for the wet sand samples nos. 129–186 as for the samples nos. 1–58. It obviously makes no sense to average the significantly different masses m_{dc} because they are not different measurements of the same quantity. It means that due to these mistakes, a statistical analysis cannot be applied to the direct measurements of m_{dc} but can lead to the final answer. Therefore, it seemed wise to replace the term $m_{w(s+c)} - m_{dc}$ in Eq. (3) by the term m_{ws}, according to Eq. (1a). This operation was possible and fully justified because the mass of the wet soil sample, m_{ws}, appeared to be normally distributed, which was certified by performing the normality tests (Shapiro-Wilk test: $W = 0.993$ and $p = 0.513 > 0.05$; d'Agostino-Pearson test: $\chi^2 = 3.034$ and $p = 0.219 > 0.05$.

The p-values presented in Table 4 and marked in green indicate a partial degradation (up to a certain acceptable level of $p > \alpha = 0.05$) in normality of the distributions, starting from m_{ws} distribution, through m_{ds} distribution, and ending up with S_r distribution, due to some subsequent steps in measuring and calculation procedures. It has to be also mentioned that the above-presented results of the normality tests take into account the existence of outliers in the individual datasets.

3.4 Probability density distribution and Q-Q plot

In statistics, the standard score or z-score is the number of standard deviations by which the value of a raw score (i.e., an observed or measured value) is above or below the mean value of what is being observed or measured. When the population mean and the population standard deviation are unknown, the standard score may be estimated by using the sample mean and sample standard deviation as estimates of the population values. In these cases, a raw score x is converted into the z-score by

$$z = \frac{x - \overline{x}}{s(x)} \tag{8}$$

It is a very common practice that the variability in a certain real-valued soil parameter, presented in the form of a histogram graphic, is compared assuming the validity of the standard normal (Gaussian) distribution, for which the probability density function is defined as (Bendat and Piersol, 1971)

$$f(x) = \frac{1}{\sqrt{2\pi}} \sim \exp\left(\frac{-z^2}{2}\right) \tag{9}$$

Respectively of the normalised histogram, it is also typical for the probability density function, given by Eq. (9), that the area under the normal distribution curve with respect to the horizontal axis equals unity. The application of Eq. (9) to the degree of saturation data leads to the normal distribution curve overlaid on the formerly established histogram (see Figure 4). A good agreement between the histogram and the theoretical curve of the normal distribution of probability is observed.

In statistics, a quantile-quantile plot, or shortly – Q-Q plot, is a graphical method commonly used to help in assessing if a set of data plausibly compares to a certain theoretical model of probability distribution. It works by comparing the quantiles of the observed (measured) data to the quantiles of a theoretical distribution. In the case of the normal (Gaussian) distribution specifically, it is usually referred to as a normal $Q - Q$ plot. Thus, in addition to the histogram presented in Figure 4, Figure 5 illustrates the normal Q-Q plot for the degree of saturation data. The ordinate axis in the Q-Q plot presents the z-score (sample data quantiles), calculated for each value of the degree of saturation according to Eq. (8), and the abscissa presents the z_p-score (normal theoretical quantiles), computed from the empirical probability obtained for the rank of the S_r values sorted in descending order and using the

Table 4. Test statistics and probability values obtained from the statistical tests on normality of the datasets representing distributions of the parameters appearing in Eq. (3).

Parameter	Shapiro-Wilk test		d'Agostino-Pearson test		$p \geq \alpha = 0.005$
	W	p-value	χ^2	p-value	
$m_{w(s+c)}$	0.990	0.220	1.758	0.415	Yes
m_{dc}	0.825	1.1×10^{-13}	23.56	7.7×10^{-6}	No
m_{ws} (Eq. (1a))	0.993	0.513	3.034	0.219	Yes
m_{ds}	0.992	0.373	2.174	0.337	Yes
G_s	0.921	0.487	0.993	0.609	Yes
S_r (Eq. (3))	0.988	0.134	3.612	0.164	Yes

inverse empirical cumulative distribution function (eCDF) to find the quantiles of the empirical distribution. The computation of the z_p-score requires the use of the probit function, which is the quantile function (the inverse of the cumulative distribution function (CDF)) associated with the standard normal distribution. The probit function can be expressed as

$$\text{probit}(p) \stackrel{\text{def}}{=} \phi^{-1}(p) = z_p = \\ = \sqrt{2}\,\text{erfc}^{-1}[1(1-p)] \tag{10}$$

where: p is the probability (or percentile in case of the empirical distribution), $\phi^{-1}(p)$ is the inverse CDF, and erfc^{-1} is the inverse complementary error function. For the purpose of the present study, the program code DIERFC.for (Ooura, 1996) was used again to compute the inverse complementary error function.

A linear regression analysis led to the determination of the best-fit trend line (red colour in Figure 5) in the Q-Q plot. The linear regression function was described by the slope $a = 0.9949$ and the z-intercept $b = -0.1418 \times 10^{-5}$. The coefficient of determination was found to be $R^2 = 0.9882$, which is very close to unity. Somewhat approximate linearity of the points in Figure 6 suggests that the degree of saturation data can be described as normally distributed. Only a few outliers are evident at the high end of the range.

Figure 5 also presents two different intervals closed between their upper and lower bands. The 95% confidence interval (bands in blue) relates to a 95% probability that the true best-fit (regression) line for the population lies within this interval. The 95% prediction interval (bands in green) illustrates the area where 95% of the z values to be found for a certain z_p value will be within the interval range around the linear regression line. In other words, if one ever uses another sample from the same population, one might find 95% z values within the prediction interval.

The vertical coordinates of the confidence bands, z_{conf}, and the prediction bands, z_{pred}, can be calculated for the horizontal coordinate, z_p, using the following equations:

$$z_{conf} = \\ = z_{reg} \pm t_{1-\alpha 2,n-2}\, SE \sqrt{\frac{1}{n} + \frac{(z_p - \overline{z_p})^2}{SS}} \tag{11a}$$

$$z_{pred} = \\ = z_{reg} \pm t_{1-\alpha/2,n-2}\, SE \sqrt{1 + \frac{1}{n} + \frac{(z_p - \overline{z_p})^2}{SS}} \tag{11b}$$

where: z_{reg} is the vertical coordinate of the linear regression line, $t_{1-\alpha/2,n-2}$ is the t-value obtained from the inverse cumulative two-tailed Student's t-distribution function for the assumed significance level α, SS is the sum of squared deviations, and SE is the standard error for the sample mean.

The significance level $\alpha = 0.05$ is a typical value assumed when constructing the confidence and prediction intervals. The t-value can be found from a t-distribution table. It can also be calculated using the significance level, α, and the number of degrees of freedom. The significance level, α, is divided by two for a two-tailed test, so the area in each tail is $\alpha/2$. In the present statistical analysis of the degree of saturation data, the t-value was equal to $t = 1.9729$ for the number of degrees of freedom $n_{df} = n - 2 = 184$ and the significance level $\alpha = 0.05(t_1 - \alpha/2) \equiv t_{0.975}$). For a large number of degrees of freedom (e.g., $n_{df} > 30$), as it is in the present study, the critical t-value can also be safely approximated by the limiting z value obtained from the inverse normal cumulative distribution function (CDF); here $t \cong z = 1.96$.

3.5 Identification of outliers

Outliers are defined as numeric values in any random data set that have an unusually high deviation from either the statistical mean or the median value. Four different methods of locating outliers were used: a) z-score method, b) Median Absolute Deviation (MAD) method, c) Tukey's Interquartile Range (IQR) method, and d) Chauvenet's criterion.

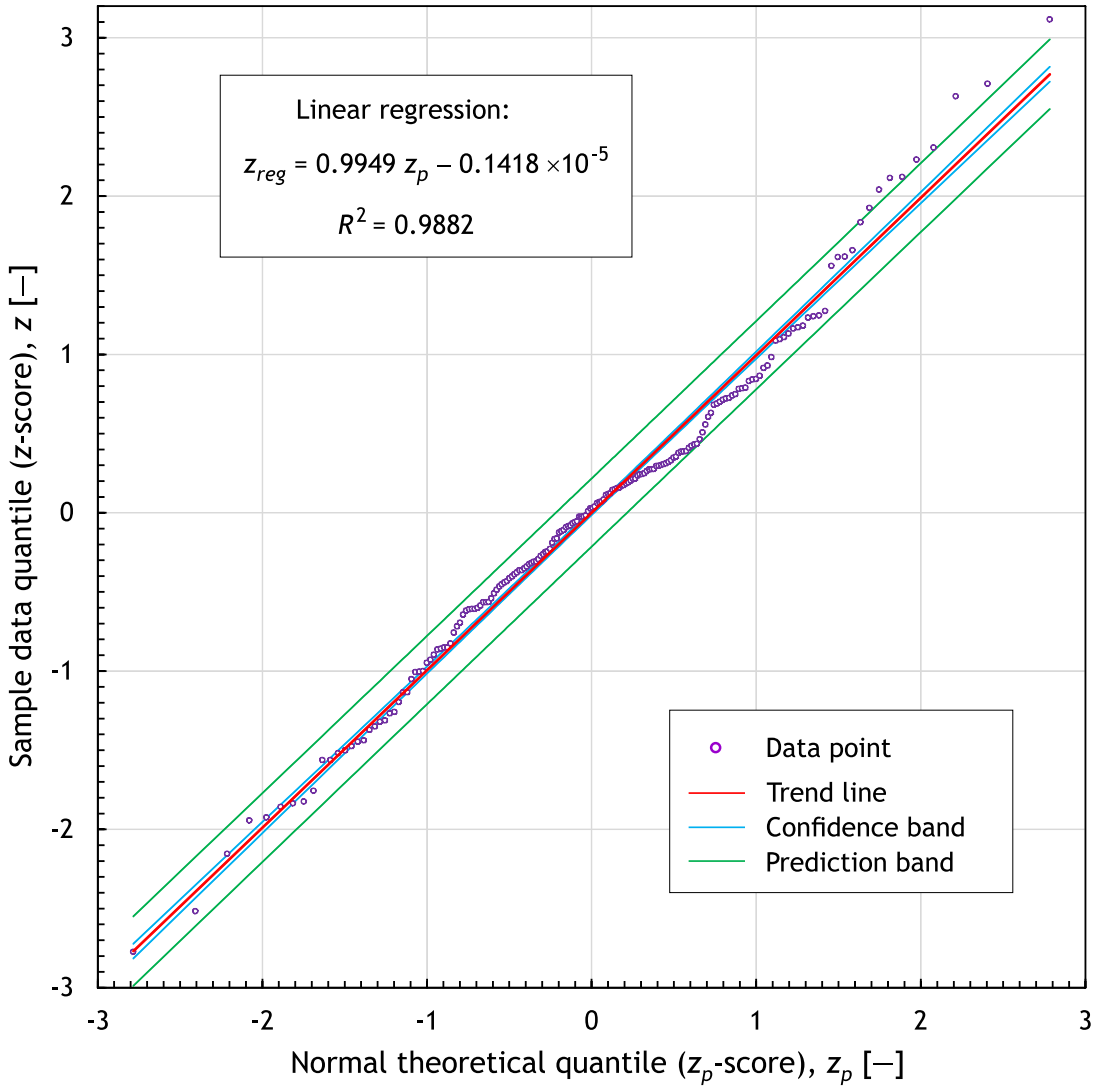

Figure 5. Normal quantile-quantile (Q-Q) plot for the degree of saturation data together with the best-fitted trend line and the confidence and prediction intervals.

The first method is rather simple. When the z-score of an observation point has a probability under 5% (confidence lever 95%, or 5% error chance), one could consider that observation an outlier. The second method is a more robust statistical technique based on the Median Absolute Deviation (MAD). Any number in a data set exceeding 3.5 times MAD is considered an outlier. In the third method, Tukey called any observation value an outlier if it is smaller than the first quartile (25%) minus 1.5 times the IQR, or larger than the third quartile (75%) plus 1.5 times the IQR. The Interquartile Range (IQR) is the width of the interval that contains the middle half of the data. Tukey's method is probably the best one in assessing outliers. The fourth method, based on Chauvenet's criterion, detects outliers by computing the absolute value of the difference between the suspected outliers and the mean divided by the sample standard deviation and comparing it with the maximum allowable deviation, which is obtained from the quantile function for the probability $p = 1 - 1/(4n)$.

Deletion of outlier data, although possible to be performed, is rather a controversial practice frowned upon by many scientists. Figure 5 presents the number of outliers identified by the above-given methods together with the associated mean values of the degree of saturation, ($\overline{S}_r$), calculated after exclusion of the outliers from the initial set of the calculated S_r values. The corrected ($\overline{S}_r$) values show very insignificant differences in relation to the mean calculated for the entire set of data ($\overline{S}_r = 0.973$). The differences vary from -0.31% (for the z-score method) to -0.10% for Chauvenet's criterion.

Removing the identified outliers from a dataset obviously improves the normality of the distribution. For exam-

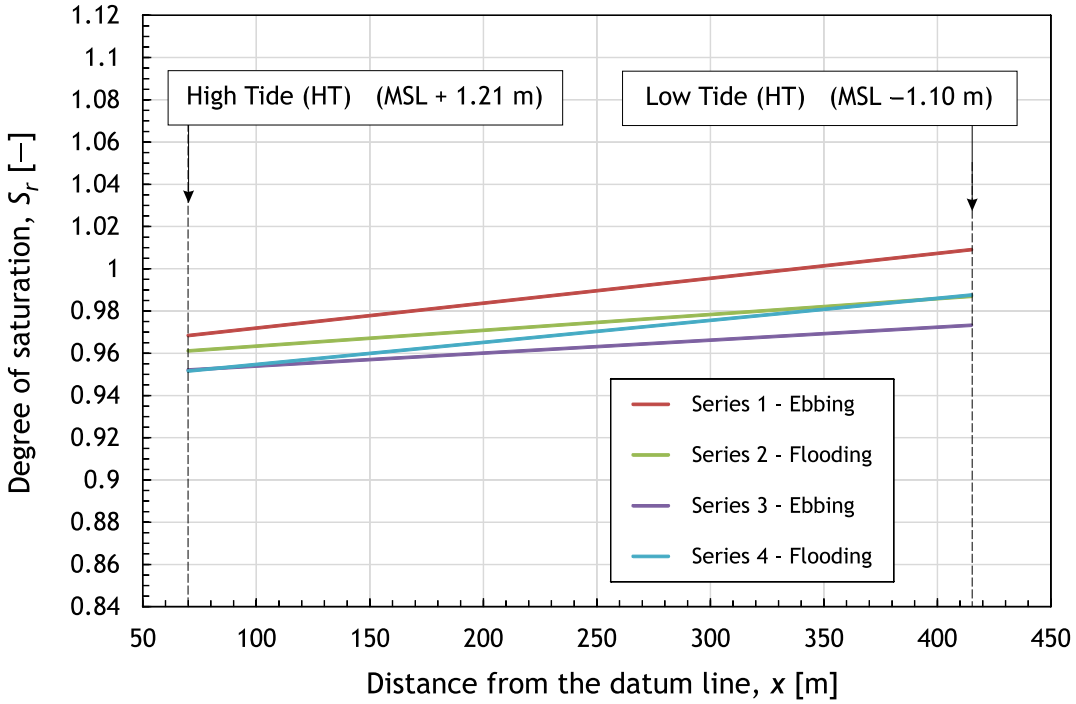

Figure 6. Trend lines for the variation of the degree of saturation, S_r, along the sampling line, calculated for four different measuring series.

Table 5. Number of potential outliers detected by different methods.

Method of identification of outliers	Number of outliers n_{out}	Percentage of outliers n_{out}/n [%]	Corrected mean of S_r $(\bar{S}_r)_{cor}$
z-score	11	5.91	0.970
Median Absolute Deviation	10	5.38	0.970
Tukey's Interquartile Range	7	3.76	0.971
Chauvenet's criterion	1	0.54	0.972

ple, eliminating 7 outliers from the dataset of the degree of saturation (as indicated by Tukey's method), the p-value increases from $p = 0.134$ (7 outliers included in the dataset) to $p = 0.338$ (7 outliers excluded from the dataset).

3.6 Propagation of uncertainties

Computing uncertainty in parameters, which are based on more complicated functions, can be done using the Law of Propagation of Uncertainty (Root Sum of Squares (RSS) method) for independent random uncertainties. After assuming independence and randomness of the variables in Eq. (3), together with the above-introduced replacement of the masses, one can use the first two terms of the Taylor series to obtain a first-order approximation of the variability in the degree of saturation. Assuming that the specific densities of pure water, ρ_w, and seawater, ρ_sw, are constant, and using the RSS method for uncertainty in a function of several variables, the following gives the differential equation for the total (complete) standard uncertainty in the degree of saturation

$$u_t(S_r) \cong \cong \sqrt{\left[\frac{\partial S_r}{\partial m_{ws}} u_c(m_w)\right]^2 + \left[\frac{\partial S_r}{\partial m_{ds}} u_c(m_{ds})\right]^2 + \left[\frac{\partial S_r}{\partial V_t} u_c(V_t)\right]^2 + \left[\frac{\partial S_r}{\partial G_s} u_c(G_s)\right]^2} \quad (12)$$

where the symbol u_c (…), together with a certain parameter symbol enclosed in round brackets, denotes the combined standard uncertainty in this parameter and can be calculated as a combination of the random (statistical) standard uncertainty (from repeated measurements), u_r, and the instrument-based (systematic) standard uncertainty (e.g., from instrument calibration, resolution, etc.), u_i, according to the following combination in quadrature

$$u_c(\ldots) = \sqrt{u_r^2(\ldots) + u_i^2(\ldots)} \quad (13)$$

Using the corrected Eq. (3), i.e. with m_{ws} instead of $m_{w(s+c)} - m_{dc}$, and applying the quotient rule of differentiation, it becomes possible to derive individual parts of

Eq. (12). The final forms of the derivatives, appearing in Eq. (12), are presented in the Appendix section (see Eqs. (A-1)–(A-4)).

When reporting the average value of n measurements, the uncertainty associated with this average value is the standard deviation of the mean, often called the standard error (SE). In order to convert an instrument's maximum uncertainty range into standard uncertainty, one has to divide the half-range by $\sqrt{3}$, assuming that a rectangular distribution of the instrument's uncertainty is valid. Therefore, for the present study, one obtains (see Table 3):

$$u_c(m_{ws}) = \\ = \sqrt{u_r^2(m_{ws}) + u_i^2(m_{w(s+c)}) + u_i^2(m_{ws})} = \\ = \sqrt{s^2(\overline{m_{ws}}) + \left(\frac{\Delta m_{w(s+c)}}{\sqrt{3}}\right)^2 + \left(\frac{\Delta m_{ws}}{\sqrt{3}}\right)^2} = \\ = \sqrt{1.71^2 + \left(\frac{0.5}{\sqrt{3}}\right)^2 + \left(\frac{0.5}{\sqrt{3}}\right)^2} = 1.76\,\text{g} \cong 2\,\text{g} \tag{14a}$$

$$u_c(m_{ds}) = \sqrt{u_r^2(m_{ds}) + u_i^2(m_{ds})} = \\ = \sqrt{s^2(\overline{m_{ds}}) + \left(\frac{\Delta m_{ds}}{\sqrt{3}}\right)^2} = \\ = \sqrt{1.67^2 + \left(\frac{0.5}{\sqrt{3}}\right)^2} = 1.69\,\text{g} \cong 2\,\text{g} \tag{14b}$$

Please note that the above-given uncertainties were rounded to one significant digit, according to the rule for stating uncertainties.

Propagation of uncertainty for several variables can be simplified considerably for the special case where the function is a simple multiplicative function of secondary variables and uncertainty is evaluated as a percentage (the so-called fractional uncertainty). Thus, taking the case of the total volume of the sample, V_t (see Eq. (5)), and using the rules for uncertainty in a measured quantity times an exact number and in a power, the instrument's uncertainty in V_t can be calculated from the following equation

$$\frac{\Delta V_t}{V_t} = \sqrt{\left(2\frac{\Delta D_i}{D_i}\right)^2 + \left(\frac{\Delta h}{h}\right)^2} \tag{15}$$

Taking into account the formerly mentioned component instrument uncertainties ($\Delta D_i = \Delta h = 0.01$ cm), the single measured dimensions of the sampling cylinder ($D_i = 9.6$ cm and $h = 12$ cm), and the calculated volume $V_t = 868.59$ cm^3, one has $\Delta V_t/V_t = 0.0022$, and finally the instrument's uncertainty $u_i(V_t) = \Delta V_t = 1.95 \cong 2$ cm^3 was obtained from Eq. (15). The random uncertainty in this single-measured parameter does not apply. Therefore, it implies that

$$u_c(V_t) = u_i(V_t) = \Delta V_t = 2\ \text{cm}^3 \tag{16}$$

In the case of the specific gravity of soil particles, G_s (see Eq. (5)), the instrument's uncertainty can also be calculated according to the RSS differential equation. Using Eq. (4), deriving appropriate derivatives, and taking the laboratory measurement results into account, the combined standard uncertainty was found to be $u_c(G_s) = 0.004$.

Finally, the total standard uncertainty in the degree of saturation can be calculated from Eq. (12). Taking the mean (best-estimated) values (see Table 3) and the respective combined standard uncertainties: $\overline{m_{ws}} = 1782.67$ g and $u_c(m_{ws}) = 2$ g, $\overline{m_{ds}} = 1472.09$ g and $u_c(m_{ds}) = 2$ g, $\overline{G_s} = 2.654$ and $u_c(G_s) = 0.004$, together with $V_t = 868.59$ cm^3 and $u_c(V_t) = 2.0$ cm^3, the total standard uncertainty in $(\overline{S_r})$ was found to be $u_t(S_r) = 0.01$. It implies that one can reasonably expect (with about 68% confidence; the coverage factor is equal to 1) that the mean value of the degree of saturation will be within the range $\overline{S_r} = 0.973\ pm\, 0.01$, which can also be written as

$$0.963 \le \overline{S_r} \le 0.983 \tag{17}$$

3.7 Influence of the annual variability of seawater conditions

The above analysis was performed, assuming the environmental seawater conditions typical for the northern coastline of Norderney during the seabed measuring campaign. These conditions were characterised by the seawater temperature $t = 6.8$°C and the practical salinity $S_p = 30$. The resultant density of seawater was calculated to be $\rho_{sw} = 1023.51$ kg/m^3. However, if one wants to spread the results of the degree of saturation over the entire annual period, it is necessary to take into account the annual mean and the seasonal variability of the sea surface temperature and salinity on the northern coast of Norderney. Based on the data from the period 1900–1996, the following values were found: $\bar{t} = 10.5$°C with $\Delta t = 7.5$°C, and $\overline{S_p} = 30$ with $\Delta S_p = 1$ (Quante and Colijn, 2016).

Using the practical formulas by Gill (1982) and Kell (1975) again, the extreme values of the density of water, influenced by temperature, pressure (the standard pressure $p_{at} = 101.325$ kPa was assumed), and salinity, were calculated, and they are as follows:

$$(\rho_{sw})_{\min} = 1020.68\ \text{kg/m}^3 \quad \begin{matrix}\text{at } t = 18°\text{C} \\ \text{and } S_p = 29\end{matrix} \tag{18a}$$

$$(\rho_{sw})_{\max} = 1024.69 \text{ kg/m}^3 \text{ at } t = 3°\text{C} \text{ and } S_p = 31 \quad (18b)$$

Accordingly, the following correction factors can be calculated:

$$(c_\rho)_{\min} = \frac{\rho_{sw}}{(\rho_{sw})_{\max}} = \frac{1023.51}{1024.69} = 0.999 \quad (19a)$$

$$(c_\rho)_{\max} = \frac{\rho_{sw}}{(\rho_{sw})_{\min}} = \frac{1023.51}{1020.68} = 1.003 \quad (19b)$$

and used by multiplying Eq. (3).

It means that the range of possible variations in $\overline{S_r}$, given in Eq. (17), must be slightly extended (by multiplying by the correction factors) due to the annual variability of the seawater temperature and salinity. Consequently, the lower range is reduced by 0.001 and the upper range is increased by 0.003, leading finally to the main result of the possible variability of the degree of saturation of the northern coastline of Norderney within the intertidal zone of water level movements

$$0.962 \leq \overline{S_r} \leq 0.986 \quad (20)$$

3.8 Tidal cycle difference in the degree of saturation

Statistical calculations for the degree of saturation, distinguishing between the 'ebbing' and 'flooding' groups of seabed samples taken during the ebbing and flooding phases of the tidal water movement, respectively, were executed. It can be emphasised that ebbing (dewatering) and flooding the beach sediments during the low tide and high tide water movements, respectively, make the degree of saturation oscillate around the mean value calculated for all 186 samples. The mean for the ebbing phase (series 1 and 3) was equal to $\overline{S_r} = 0.974$, and for the flooding phase $\overline{S_r} = 0.972$; the difference is practically negligible.

An even more interesting observation is that the spatial distribution of S_r along the sampling line has an increasing tendency when moving from the high tide (HT) line towards the low tide (LT) line, irrespective of the series of sampling (ebbing or flooding). The maximum and minimum differences in S_r were found to be +0.041 (series 1) and +0.021 (series 3), respectively. This particular finding is confirmed in Figure 6, presenting the results of the additional spatial analysis obtained in terms of the best-fit trend lines for the variation of the degree of saturation along the sampling line. Qualitatively, these results were expected and they can have a twofold explanation. Firstly, during the flooding period, the wet seabed sediments entrap small amounts of air within the soil voids and, consequently, the degree of saturation is slightly lower than that obtained during the ebbing phase. Although water filtrates faster in wet sands than in dry sandy sediments, it seems that the horizontal velocity of flooding (345 m/6 h $\cong$ 0.016 m/s) evidently dominates the vertical groundwater velocity (2.31 m/6 h $\cong 10^{-4}$ m/s, which is quite comparable with the coefficient of permeability of fine sand $k \cong 10^{-4}$ m/s). Secondly, the lower areas of the beach within the intertidal zone remain below the water surface longer and are subjected to wave action longer than the upper parts of the beach. This strongly affects the bottom and causes significant oscillatory movements of the bottom sediments, leading to some release of the air entrapped in the soil in the form of microscopic occluded bubbles during the flooding phases of the tidal water movement.

In addition to the graphical presentation, statistical testing by using an unpaired t-test (or independent samples t-test) seems to be appropriate as a statistical tool used to compare the means of two separate, unrelated groups to check if there is a statistically significant difference between them. In other words, the testing should determine whether observed differences are due to chance (random) or a real effect, with results assessed by a calculated statistic t-value and a probability p-value. In the case of unequal variances, the Welch's t-test is widely used and more reliable than the Student's t-test, which is better when variances are assumed equal. The main assumptions for the t-test performance are: observations within and between groups are independent, data in each group should be approximately normally distributed, and the variances of the two groups should be roughly equal. The input data required for the t-test are collected in Table 6, and the results of the Welch's t-test are presented in Table 7.

Assuming the significant level $\alpha = 0.05$, it can be concluded that the condition $p \geq \alpha = 0.005$ is fulfilled in all the considered cases. It means that the differences between the means of the degree of saturation, found for the complementary phases (ebbing and flooding) of one full tidal cycle of the water movement, are not big enough to be statistically significant. The existing small differences could happen by chance and, therefore, have a random character.

3.9 Comments on the degree of saturation above unity

When reviewing the calculated saturation degrees, it was found that some of them (44 of 186 tests, or 23.7% of all tests) exceed unity. From a physical point of view, it is impossible to have a degree of saturation $S_r > 1$. However, from an engineering point of view, this result is not so much surprising because of the nature of the sampling procedure, the undoubted random variability of measurements, and a certain inhomogeneity of seabed sediments. It has to be noted that even after introducing the most inconvenient combination of the instrument's uncertainties into Eq. (3), lowering thereby the S_r values as much as possible, there are still 25 tests (15.0% of all tests) remaining with

Table 6. Statistical values related to the degree of saturation, S_r, and calculated exclusively for the seabed samples taken during the ebbing or flooding phases of the tidal water movement.

Phases of tidal water movement	Number of data n	Mean $\overline{S}_r$	Standard deviation $s(S_r)$
Series 1 (ebbing)	38	0.989	0.057
Series 2 (flooding)	40	0.974	0.028
Series 3 (ebbing)	49	0.963	0.043
Series 4 (flooding)	59	0.970	0.034

Table 7. Results of the Welch's t-test for all possible combinations of the seabed sampling series, reflecting one tidal ebbing-flooding cycle of the water movement.

Merged phases of tidal water movement	Statistic t-value	Probability p-value	$p \geq \alpha = 0.005$?
Series 1 + 2	1.426	0.160	Yes
Series 1 + 4	1.859	0.069	Yes
Series 2 + 3	1.489	0.140	Yes
Series 3 + 4	0.915	0.363	Yes

$S_r > 1$. It certifies that both types of uncertainties (random and instrument), related to sampling disturbances and measurement errors, influence the degree of saturation in exceeding unity. It is also believed that a natural variability (inhomogeneity) of S_r influences the results, but this cannot be clarified quantitatively at the present stage of the research.

According to Schmertmann (1989), rejecting tests with $S_r > 1$ would distort statistical findings from the field sampling and may have important engineering and economic consequences. He performed an excessive statistical analysis of the data gained from the density check conducted at three fills. In his 31 tests (17% from the total number of 187 tests), the degree of saturation was reported to have values above unity ($S_r > 1$), although the mean was equal to $\overline{S}_r = 0.877$. Applying the so-called Zero Air Voids Line (ZAVL) approach, Schmertmann (1989) demonstrated that one should expect a certain percentage of all random tests to compute with $S_r > 1$, that this percentage increases with the mean degree of saturation, $\overline{S}_r$, and that any such tests have as much validity as the tests with $S_r \leq 1$. After all, it should be clear to everyone that any approximately symmetrical distribution of variability around the mean $\overline{S}_r = 1$ would produce approximately one half of the computed S_r values higher than the mean ($S_r > \overline{S}_r = 1$), and if one eliminates the tests with $S_r > 1$ from the dataset statistical processing, the mean will be artificially corrupted and lower than unity. In the present study, the elimination of 44 values of $S_r > 1$ from the entire dataset would lead to the mean equal to $\overline{S}_r = 0.955$. This action, however, destroys the normality of S_r distribution, which is certified by the statistic $W = 0.922$ and the probability value $p = 10^{-7} < \alpha = 0.05$ obtained from the Shapiro-Wilk normality test.

From the formerly proven assumption of the normally distributed values of the degree of saturation, it becomes possible to calculate the expected percentage of tests with $S_r > 1$ using the following formula

$$P(S_r > 1.0) = \\ = \frac{1}{s(S_r)\sqrt{2\pi}} \int_{1.0}^{\infty} \exp\left\{-\frac{(1.0-\overline{S}_r)^2}{2[s(S_r)]^2}\right\} dS_r \qquad (21)$$

In the present study, this calculation was performed numerically where the procedure of numerical integration, using the extended midpoint rule programmed in subroutine MIDINF (Press et al., 1992), had to be implemented because the integral to be calculated is an improper integral, the upper limit of which approaches infinity (see Eq. (21)). Using Eq. (21), taking the standard deviation $s(S_r) = 0.045$ and the mean $\overline{S}_r = 0.973$ (see Table 3), the analytically evaluated percentage of tests with the degree of saturation exceeding unity was calculated to be 27.4%, compared to 23.7% of values calculated from the field sampling, laboratory measurements, and the use of Eq. (3). This rather small discrepancy can be explained by small differences between the theoretical normal distribution of probability and the experimental normalised distribution of the degree of saturation illustrated in the histogram (see Figure 4).

4. Conclusion

Any information on real saturation conditions of seabed sediments is hard to find in the professional literature. Therefore, a measuring campaign performed on the intertidal region of the northern coast of Norderney created a very unique possibility to obtain realistic characteristics of the degree of saturation. After the in-situ sampling of the seabed on Norderney, followed by appropriate laboratory measurements of 186 sand samples, a thorough statistical analysis of the measured data was performed. Treating the measured soil parameters as real-valued random variables, and using two different normality tests (Shapiro-Wilk test and d'Agostino-Pearson test) together with the histogram and the Q-Q plot, the assumption of the normal (Gaussian) distribution of probability in application to the variability in the degree of saturation, calculated from the measured masses of the seabed samples, was proved. The mean value of the degree of saturation was found to be $\overline{S}_r = 0.973$, whereas a possible range of variation in $\overline{S}_r$, equal to 0.962–0.986, was calculated based on the analysis of propagation of uncertainties (both random and instrumental), and taking into account the annual variabilities

of the seawater temperature and salinity, influencing the seawater density.

This outcome obviously has important consequences for coastal engineering practice. The values of the degree of saturation, obtained from the intertidal range of the seabed, are believed to create the lower limit for S_r values typical for seabeds, which are totally and continuously submerged. On the other hand, it must be strongly emphasized that the obtained mean value $\overline{S}_r = 0.973$ is larger, sometimes much larger, than the values used to this day by many coastal engineers and researchers, thereby putting into question their theoretical results of different analytical and numerical analyses of the wave-induced cyclic seabed response.

Another interesting finding is related to the spatial distribution of the degree of saturation along the sampling line set perpendicular to the coastline. The present research indicated an increasing tendency of S_r distribution when moving from the high tide line towards the low tide line, regardless of the direction of sampling, i.e., during the ebbing or flooding phases of the tidal water movement. By performing the Welch's t-test, it was proved that there is no significant difference between the means of the degree of saturation, calculated for the ebbing and flooding phases of the tidal cycle of water movements. The reported changes in S_r within the intertidal zone could be of some engineering interest as far as the design of submarine pipelines buried in seabed sediments is concerned. This is due to a strong influence of the seabed saturation conditions on the pore-fluid pressure field around a buried coastal structure.

Of course, one has to remember that seabed sediments can be characterised by much lower values of S_r than the values obtained from the present study. However, this can happen only due to methane deposits existing along the seabed in deep-water regions, and this exceptional case was of no interest in the present paper.

Acknowledgements

The author of the present paper is grateful for the financial support of The German Research Foundation (in German: Deutsche Forschungsgemeinschaft (DFG)) addressed to the research programme TP-A13 'Cyclic and transient wave-induced loading of the seabed' (in German: 'Transiente und zyklische Beanspruchung von Böden durch Seegang') within the frame of the Coastal Engineering Research Programme (in German: Sonderforschungsbereich – 205 'Küsteningenieurwesen' (SFB-205)).

First of all, the author would like to express very warm words of thanks to Professor Werner Richwien, who was responsible for the implementation and the day-to-day management of the scientific programme TP-A13 within the SFB-205, for his scientific leadership and substantial help in organising the measuring campaign on Norderney.

The author also wishes to appreciate the great engagement, technical support and practical advice of Mr. Herbert Seehausen and Mr. Adolf Adam in organising the expedition and performing in-situ sampling and all the laboratory testing and measurements.

The author is very obliged to Prof. Hanz Kunz – the head of the Research Coastal Station on Norderney (in German: Niedersächsischer Landesbetrieb für Wasserwirtschaft, Küsten- und Naturschutz (NLWKN) – Forschungsstelle Küste (FSK)) and his co-worker Dr. Günther Ragutzki for their great help by giving permission for seabed sampling and supplying with a scientific consultation and great laboratory facilities.

Conflict of interest

None declared.

References

Bendat, J.S., Piersol, A.G., 1971. *Random Data: Analysis and Measurement Procedures*. John Wiley & Sons, Inc., 200 pp.
https://ia801506.us.archive.org/15/items/in.ernet.dli.2015.134197/2015.134197.Random-Data-Analysis-And-Measurement-Procedures.pdf

Craig, R.F., 2004. *Craig's Soil Mechanics*. Seventh edition, Spon Press, Taylor & Francis Group, London, New York, 460 pp.
https://doi.org/10.4324/9780203494103

Eichmanns, C., Schüttrumpf, H., 2021. *Influence of sand trapping fences on dune toe growth and its relation with potential aeolian sediment transport*. J. Marine Sci. Eng. (MDPI) 9, 850, 1–30.
https://doi.org/10.3390/jmse9080850

Fox, J., 2016. *Applied Regression Analysis and Generalized Linear Models*. SAGE Publ. Inc., Los Angeles (3rd edn.), 791 pp.
https://dokumen.pub/applied-regression-analysis-and-generalized-linear-models-3nbsped-1452205663-9781452205663.html

Gill, A.E., 1982. *Atmosphere-Ocean Dynamics*. Int. Geophys. Ser. 30. Acad. Press, San Diego, Ca., London, 662 pp.
https://archive.org/details/AtmosphereOceanDynamicsGill

Hsu, J.R.C., Jeng, D.S., 1994. *Wave-induced soil response in an unsaturated anisotropic seabed of finite thickness*. Int. J. Numer. Anal. Meth. Geomech. 18, 785–807.
https://doi.org/10.1002/nag.1610181104

Jeng, D.S., 2013. *Porous Models for Wave-seabed Interactions*. Springer, Heidelberg, New York Dordrecht London, 289 pp.
https://doi.org/10.1007/978-3-642-33593-8

Jeng, D.S., 2018. *Mechanics of Wave-Seabed-Structure Interactions. Modelling, Processes and Applications*. Cam-

bridge University Press, Cambridge, 358 pp. https://doi.org/10.1017/9781316672266

Kell, G.S., 1975. *Density, thermal expansivity, and compressibility of liquid water from 0°C to 150°C: correlations and tables for atmospheric pressure and saturation reviewed and expressed on 1968 temperature scale*. J. Chem. Eng. Data 20, 97–105. http://http://www.bioconsult.ch/Inovatech/W-Lehre/J+Che+Eng+Dat20,+97.pdf

Madsen, O.S., 1978. *Wave-induced pore pressures and effective stresses in a porous bed.* Géotechnique 28, 377–393. https://doi.org/10.1680/geot.1978.28.4.377

Magda, W., 1992. *Wave-induced pore pressure acting on a buried submarine pipeline*. Proc. 23th Conf. Coas. Eng. (ICCE 1992), Am. Soc. Civil Eng. 4–9 October 1992, Venice, Italy, 3135–3148. https://doi.org/10.1061/9780872629332.239

Magda, W., 1994. *Analytical solution for the wave-induced excess pore-pressure in a finite-thickness seabed layer*. Proc. 24th Conf. Coast. Eng. (ICCE 1994), ASCE, 23–28 October 1994, Kobe, Japan, 3111–3125. https://doi.org/10.1061/9780784400890.225

Magda, W. 1997. *Wave-induced uplift force on a submarine pipeline buried in a compressible seabed*. Ocean Eng. 24(6), 551–576. https://www.sciencedirect.com/science/article/abs/pii/S0029801896000315

Magda, W., 1998. *Wave-Induced Pore Pressure Oscillations in Sandy Seabed Sediments*. Ph.D. thes., Tech. Univ. Gdańsk, Marine Civil Eng. Depart., Gdańsk, Poland, 170 pp. https://mostwiedzy.pl/pl/publication/wave-induced-pore-pressure-oscillations-in-sandy-seabed-sediments,75377-1

Magda, W., 2000. *Wave-induced cyclic pore-pressure perturbation effects in hydrodynamic uplift force acting on submarine pipeline buried in seabed sediments*. Coast. Eng. 39(2–4), 243–272. https://www.sciencedirect.com/science/article/abs/pii/S0378383999000630

Magda, W., 2025. *Criticism of the analytical solutions to the wave-induced cyclic response of a poro-elstic seabed of finite thickness*. Arch. Hydro-Eng. Environ. Mech. 72(1), 51–74. https://doi.org/10.2478/heem-2025-0004

Mei, C.C., Foda, M.A., 1981. *Wave-induced responses in a fluid-filled poroelastic solid with a free surface – a boundary layer theory*. Geophys. J. Royal Astronom. Soc. 66, 597–631. https://doi.org/10.1111/j.1365-246X.1981.tb04892.x

Merxhani, A., Liang, D., 2012. *Investigation of the poro-elastic response of seabed to solitary*. Proc. 22nd (2012) Int. Offshore Polar Eng. Conf., Rhodes, Greece, June 17–22, 2012, 101–108. https://onepetro.org/ISOPEIOPEC/proceedings-abstract/ISOPE12/ISOPE12/ISOPE-I-12-433/12908?redirectedFrom=PDF

Michallet, H., Mory, M., Piedra-Cueva, I., 2009. *Wave-induced pore pressure measurements near a coastal structures*. J. Geophys. Res. 114(C06019), 1–18. https://doi.org/10.1029/2008JC005071

Nago, H., Maeno, S., 1984. *Pore water pressure in sand bed under oscillating water pressure*. Memoirs School Eng., Okayama Univ., Tsushima, Okayama, Japan. https://files01.core.ac.uk/download/pdf/12528934.pdf

Niemeyer, H.D., 1992. *Die ursächliche Deutung van Transpanphänomenen als Gestaltungsgrundlage für Strandauffüllungen*. [In:] Die Küste 54, 53–92. Heide, Holstein, Boyens. https://henry.baw.de/items/c00bb39e-4230-41fa-9f00-047a9f15a341

Okusa, S., 1985. *Wave-induced stresses in unsaturated submarine sediments*. Géotechnique 35, 517–532. https://doi.org/10.1680/geot.1985.35.4.517

Ooura, T., 1996. *Gamma and Error functions*. Computer codes in C and Fortran. https://www.kurims.kyoto-u.ac.jp/~ooura/gamerf.html

Press, W.H., Teukolsky, S.A., Vetterling, W.T., Flannery, B.P., 1997. *Numerical Recipes in Fortran 77. The Art of Scientific Computing*, Fortran Numerical Recipes Vol. 1, Cambridge Univ. Press, 973 pp. https://belglas.com/wp-content/uploads/2019/10/numericalrecipesinf77.pdf

Quante, M., Colijn, F, 2016. *North Sea Region Climate Change Assessment,* Springer Nature, 528 pp. https://link.springer.com/book/10.1007/978-3-319-39745-0

Richwien, W., Magda, W., 1994. *Design Levels For Offshore Structure. State-of-the-Art and Instantenous Pore-Pressure Model*. Forschungsbereich aus dem Fachbereich Bauwesen, Universität, Heft 63, Gesamthochschule Essen, Essen, 103 pp. https://cloud.wilis.pg.edu.pl/index.php/s/PsLTJzk4CMrAEED

Royston, P., 1982. *An extension of Shapiro and Wilk's W test for normality to large samples*. J. Royal Stat. Soc. Ser. C 31(2), 115–124. https://www.jstor.org/stable/2347973

Sandven, R., Husby, E., Husby, J.E., Jönland, J., Roksvåg, K.O., Staehli, F., Tellugen, R., 2007. *Development of a sampler for measurement of gas content in soils*. J. Water. Port Coast. Ocean Eng. 133(1), 3–13. https://ascelibrary.org/doi/abs/10.1061/%28ASCE%290733-950X%282007%29133%3A1%283%29

Schmertmann, J.H., 1989. *Density tests above zero air voids line*. J. Geotech.Eng. 115, 1003–1018. https://doi.org/10.1061/(ASCE)0733-9410(1989)1

15:7(1003)
Sumer, B.M., 2014. *Liquefaction Around Marine Structures*, World Scientific, New Jersey, 472 pp. https://doi.org/10.1142/7986
Tørum , A., 2007. Wave-induced pore pressures Air/gas content. J. Water. Port Coast. Ocean Eng. 133(1), 83–86. https://ascelibrary.org/doi/10.1061/(ASCE)0733-950X(2007)133%3A1(83)
Ulker, M.B.C., Rahman, M.S., 2009. *Response of saturated and nearly saturated porous media: Different formulations and their applicability*. Int. J. Numerical Analy. Methods Geomech. 33(5), 633–664. https://doi.org/10.1002/nag.739
Verruijt, A., 1969. *Elastic storage of aquifers*. [In:] R. J. M. DeWiest, (ed.), *Flow Through Porous Media*, Acad. Press, New York, London, 331–376. https://www.researchgate.net/publication/258354880
Wikipedia.com, 2025. *Norderney*. https://pl.wikipedia.org/wiki/Norderney
Yamamoto, T., Koning, H.L., Sellmeijer, H., Hijum, E., 1978. *On the response of a poro-elastic bed to water waves.* J. Fluid Mech. 87, 193–206. https://doi.org/10.1017/S0022112078003006

Appendix

Partial derivatives of Eq. (3), obtained with respect to the component parameters (ρ_w and ρ_{ws} are assumed to be constant), are as follows:

$$\frac{\partial S_r}{\partial m_{ws}} = \frac{1}{\rho_w V_t - \frac{m_{ds}}{G_s}} \times \frac{\rho_w}{\rho_{sw}} \tag{A-1}$$

$$\frac{\partial S_r}{\partial m_{ds}} = \frac{-\rho_w V_t + \frac{m_{ws}}{G_s}}{\left(\rho_w V_t - \frac{m_{ds}}{G_s}\right)^2} \times \frac{\rho_w}{\rho_{sw}} \tag{A-2}$$

$$\frac{\partial S_r}{\partial V_t} = \frac{-(m_{ws} - m_{ds})\rho_w}{\left(\rho_w V_t - \frac{m_{ds}}{G_s}\right)^2} \times \frac{\rho_w}{\rho_{sw}} \tag{A-3}$$

$$\frac{\partial S_r}{\partial G_s} = \frac{-(m_{ws} - m_{ds})\frac{m_{ds}}{G_s^2}}{\left(\rho_w V_t - \frac{m_{ds}}{G_s}\right)^2} \times \frac{\rho_w}{\rho_{sw}} \tag{A-4}$$